applied sciences

MDPI

Article

Design and Construction of Oblique Prestressed Concrete Pavement: A Case Study in China

Ling Yu [1], Xu Yang [2,*], Xiaohui Yan [3,†], Xiaowei Zhang [1,†], Ting Zhao [4,†], Cong Duan [5] and Julian Mills-Beale [6]

1 School of Transportation, Shenyang Jianzhu University, East Hunnan Road, Shenyang 110168, China; 13516094255@163.com (L.Y.); 18698277088@163.com (X.Z.)
2 Department of Civil Engineering, Monash University, Clayton VIC 3800, Australia
3 Henan Vocational College of Water Conservancy and Environment, Garden Street, Zhengzhou 450008, China; 406779136@163.com
4 Department of English for Nonmajors, Shenyang Jianzhu University, East Hunnan Road, Shenyang 110168, China; ztjoseph2018@163.com
5 National Land Resources Engineering Institute, Lianhua Campus, Kunming University of Science and Technology, Kunming 650093, China; dcworkhard@163.com
6 Department of Civil & Environmental Engineering, California Baptist University, 8432 Magnolia Ave, Riverside, CA 92504, USA; jmillsbe@calbaptist.edu
* Correspondence: xu.yang@monash.edu
† These authors contributed equally to this work.

Received: 11 February 2018; Accepted: 5 April 2018; Published: 11 April 2018

Featured Application: This paper introduced a practical application of oblique prestressed concrete pavement in China. The design and construction experience of this study can provide useful information for the prestressed concrete pavement in other regions of China as well in as other countries.

Abstract: Prestressed concrete pavement can reduce slab thickness, eliminate transverse joints and enhance durability compared to traditional concrete pavement. Traditional prestressing or precast prestressing in the longitudinal direction requires additional space for anchorage and adds more joints. This study proposed an oblique prestress concrete pavement, in which prestressed tendons were distributed with an angle to the road direction so that the prestress can be applied in both the transverse and longitudinal directions. The detailed design of the oblique prestress concrete pavement, including the selection of raw materials, design of cement concrete, anchorage area, size and distribution of prestressed tendons, stress analysis within the concrete slab, sliding layer, side reinforcement, and regular reinforcement at top and bottom are all included in this study. The slab thickness, diameter, distribution angle, and spacing of tendons were obtained based on the stress analysis to meet the requirement of fracture criteria and fatigue criteria. A demonstrative road pavement section, which has performed well after three years of traffic opening, was constructed according to the design. A step-by-step description of the construction was also presented in the study.

Keywords: prestressed concrete pavement; oblique; demonstrative road section; stress analysis

1. Introduction

The earliest application of prestressed concrete pavement was in as early as the 1940s. Prestressed concrete pavements have been constructed for highways and airfields in Europe and the United States since then [1]. Some basic geometrical and economical designs of prestressed concrete pavement have also been reported [2–4]. The benefits of prestressed concrete pavement include improved cracking

resistance and reduced slab thickness; while the prestressing increases the cost of the materials and construction, the reduction in slab thickness and transverse joints can compensate some of this cost [1,5,6]. According to El-Reedy, the prestressed concrete slab with 200 mm thickness can possess equivalent design life as the traditional concrete slab with 355 mm thickness [7]. In another airfield runway study, it was determined that the thickness of the concrete slab can be reduced by half when prestressing is applied [8].

Generally, there are two types of prestressed concrete pavement: cast-in-place and precast. In the cast-in-place method, concrete slabs are constructed on-site, and the prestressing is applied either before or after construction. The most widely used prestressing approach is post-tensioning in the longitudinal direction in the early stage [9]. This technique requires some space for the anchorage area at the two ends of the slabs. Additionally, this type of prestressing limits the length of concrete slab because the prestressing loss would be high if the concrete slab is long. Due to prestressing loss, another prestressing method, known as cross tensioned, concrete pavement was introduced [1]. In the cross tensioned method, the prestressed tendons are distributed obliquely with an angle in the road direction so that the prestressing can be applied in both transverse and longitudinal directions. By adjusting the angle, the proportion of prestressing in the transverse and longitudinal directions can be changed. The prestressing in the transverse direction provides lateral constraints to the slab so that the transverse joints can be eliminated [10]. The anchorage area is on the side of the concrete slabs so that long concrete slabs can be achieved without sacrificing the prestressing [10–12].

A sliding layer between the base layer and the prestressed concrete slab is necessary to reduce the friction during the tensioning. Han et al. reported that the sliding layer can reduce the stress and deformation resulting from longer concrete slabs [11]. They proposed a design for the sliding layer with sand, cement, and polyethylene-plastic sheeting. However, the prestressed concrete pavement may be still prone to cracks if the underneath base layer is not flat [11,13]. Cement grout may be injected underneath the prestressed concrete slabs to compensate for the settlement of the ground. However, pulverization may occur due to repeated traffic loading in some cases [14].

Precast prestressed concrete pavement has been developed recently for the purpose of rapid pavement construction and rehabilitation. Compared to the cast-in-place method, the precast method can reduce construction time and improve durability [15]. The construction speed can be increased by two to three times if using the precast method instead of the case-in-place method [15]. The United States has been encouraging the application of precast prestressed concrete pavement in state highways and many demonstration sections have been constructed. While the long-term performance of prestressed concrete pavement has not been seen yet, the early-age performance indicates that it has a great potential to be used as a rapid construction or rehabilitation material [5].

In the precast prestressing concrete pavement, the prestressing is applied in the longitudinal direction, transverse direction, or both directions. Different tensioning methods have been reported in existing literatures. Transverse prestressing was applied on concrete slabs in the study by Syed and Sonparote [16]. A transverse pre-tensioning was applied during the concrete slab fabrication and a longitudinal post-tensioning was applied after the installation on the road [17]. In another study, the post-tensioning was conducted in both the transverse and longitudinal directions after the fabrication of the concrete slab [18]. The size of the precast concrete slab is relatively low. For instance, the panel size in the study by Syed and Sonparote was 3.5 × 4.5 m, and that in the study by Qu et al. was 1.5 × 1.5 m [16,18]. Special designs may be needed at the joints to help the load transfer of neighboring slabs. While the driving experience of precast prestressed concrete pavement has not been reported in existing literatures, the large amount of joints may impact driving comfort.

Finite element analysis has been applied to model the temperature and load stresses as well as mechanical responses of prestressed concrete pavement [19,20]. Naddafi and Sadeghi pointed out that a high prestressing force may impact the load transfer within concrete pavement and suggested using caution with prestress higher than 400 kN [20]. Kim et al. showed that the variation in base or subbase layers had a minimal effect on the maximum induced stresses in the precast prestressed concrete

pavement via a finite element analysis [21]. Finite element analysis has also been used to find the most critical areas within the concrete slab and help the design of prestressed concrete pavement [1]. Fatigue damage is the most common distress type of prestressed concrete pavement; this distress can be detected by Fourier and wavelet analysis [10,22]. The critical stresses were found at the panel edges due to the combination of temperature stresses and traffic loading [16].

Although the cross tensioned concrete pavement has been introduced in some previous literatures, the detailed design, construction, and demonstration project have not been well reported. The influential factors that significantly affect the stress level within the concrete slab have been rarely explored. This paper aims to present the detailed design and construction of cross tensioned concrete pavement, and includes raw material selection, stress analysis, concrete design, tendon selection and distribution, tendon spacing, sliding layer design, anchorage design, and construction. This study will provide a detailed explanation of how prestressed concrete pavement is designed and constructed.

2. Methodology

Prestressed concrete pavement as a composite structure should be properly designed before implementation. The design should take traffic condition, or cumulative equivalent axle repetitions in the service life, into account, and the dimension of the concrete slab should be determined (the dimension should meet the requirement specified in the code of the prestressed concrete pavement in China [23]). The cement concrete should also be properly designed with enough workability and strength. The prestressed concrete tendons should be selected and the distribution (direction and spacing) of the tendons can be tentatively determined. A stress analysis may be conducted to verify the distribution of prestressed tendons. If the concrete's internal stress is not higher than the design strength of the concrete, the distribution of the prestressed tendons is acceptable. After determining if the stress is acceptable, the anchorage area and the regular reinforcement using steel bars should be designed. A stress analysis should also be carried out to verify the design. The design procedure of the prestressed concrete pavement is described in Figure 1.

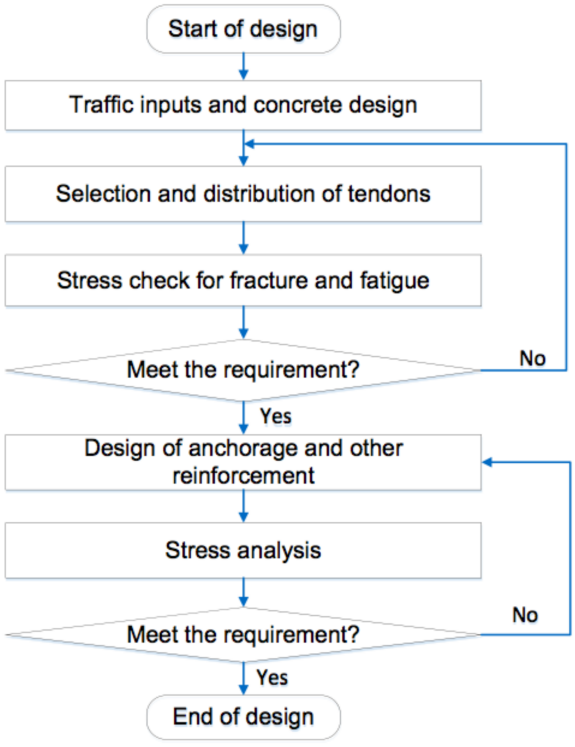

Figure 1. Design procedure of prestressed concrete pavement.

3. Stress Analysis of Oblique Prestressed Concrete Slabs

3.1. Prestress Loss

According to the specification of unbonded prestressed concrete structure, the effective stress of the oblique prestressed tendons can be expressed as [24]:

$$\sigma_{pe} = \sigma_{con} - \sum_{n=1}^{5} \sigma_{ln} \tag{1}$$

where,

σ_{pe} = the effective stress;
σ_{ln} = the value of prestress loss of item n (n = 1 to 5);
σ_{con} = the tensioned control stress of prestressed reinforcement.

In general, the prestress loss include the following four aspects [24,25]:

(1) Prestress loss caused by the anchorage deformation and the shrinkage when tensioning the prestressed reinforcement, denoted as σ_{l1}. Regardless how the tendons are tensioned, the deformation of anchorage and the base plate, as well as the sliding of the prestressed tendons can cause prestress loss. The prestress loss due to the tendon shrinkage mainly occurs around the anchorage area and is non-uniform along with the tendon direction [26]. The prestress loss due to anchor deformation and tendon shrinkage can be calculated as:

$$\sigma_{l1} = \frac{a}{l} E_p \tag{2}$$

where,

σ_{l1} = the prestress loss due to anchor deformation;
l = the distance between the two anchor ends, mm;
a = the shrinkage length of the tendons due to anchor deformation, for jaw vice anchorage, 6–8 mm.

(2) Prestress loss due to friction, denoted as σ_{l2}. There is friction between the prestressed tendons and the casing pipe. The closer to the anchorage area, the higher is the friction force, which can be expressed as [24]:

$$\sigma_{l2} = \begin{cases} \sigma_{con}\left(1 - e^{-(kx+\mu\theta)}\right) & kx + \mu\theta > 0.2 \\ \sigma_{con}(kx + \mu\theta) & kx + \mu\theta \leq 0.2 \end{cases} \tag{3}$$

where,

σ_{l2} = the prestress loss due to friction;
x = the distance from the anchorage area to the calculation cross section;
k = the factor of the casing pipe;
μ = the friction coefficient between the tendons and the casing pipe;
θ = the cumulative angle.

(3) Prestress loss due to relaxation. The unrecovered deformation of steel wires at high tensioning is inevitable, which is also known as relaxation. The prestress loss due to this can be expressed as [24]:

$$\sigma_{l3} = 0.125\left(\frac{\sigma_{con}}{f_{ptk}} - 0.5\right)\sigma_{con} \tag{4}$$

where,

$$0.7 f_{ptk} < \sigma_{con} < 0.8 f_{ptk}$$

σ_{l3} = the prestress loss due to relaxation;
f_{ptk} = the tensile strength of the prestress tendons.

(4) Prestress due to concrete shrinkage and creep. Shrinkage is a common phenomenon during the curing of concrete. Creep occurs when high pressure is applied on the concrete. Both the shrinkage and creep can cause prestress loss, which can be expressed as [24]:

$$\sigma_{l3} = \frac{35 + 280\frac{\sigma_{pc}}{f'_{cu}}}{1 + 15\rho} \tag{5}$$

where,

ρ = the reinforcement ratio;
σ_{pc} = the normal compressive stress of concrete;
f'_{cu} = the compressive strength of concrete under pressure.

3.2. Longitudinal and Transverse Stress

Figure 2 shows an example of the oblique prestressed concrete slab. Both transverse and longitudinal compressive stresses will be applied on the concrete due to the prestressing. The longitudinal and transverse stresses can be expressed as:

$$\sigma_{pL} = \frac{2(\sigma_{con} - \sigma_l)A_p cos(\alpha)}{h \cdot l \cdot tan(\alpha)} \tag{6}$$

$$\sigma_{pT} = \frac{2(\sigma_{con} - \sigma_l)A_p sin(\alpha)}{h \cdot l} \tag{7}$$

where,

σ_{pL} = the longitudinal prestress;
σ_{pT} = the transverse prestress;
σ_{con} = the controlled design strength of tendons;
A_p = the cross section area of the prestressed tendons;
l = the spacing between neighboring tendons along the road direction;
h = the thickness of the concrete slab.

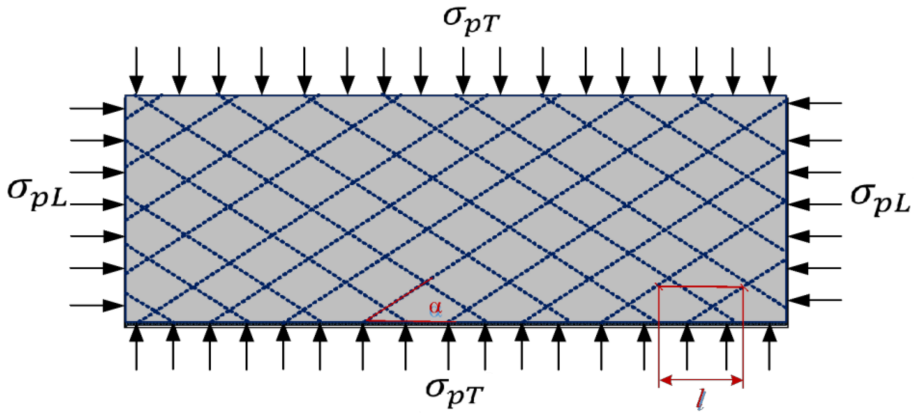

Figure 2. A sample concrete slab with transverse and longitudinal stress under oblique prestressed reinforcement.

According to Equations (6) and (7), the cross-sectional area of tendon (A_p), thickness of concrete slab (h), the distribution angle (α), and the spacing (l) are the main influential factors affecting the

stress distribution and level within the concrete slab. Thus, a parametric study was carried out to quantify the effect of these factors on the stress in the concrete slab. The once-at-a-time method was used to analyze the effect of individual factors. Some tentative values for the factors were selected based on the specification and the typical local concrete design. The slab thickness was set as 20 cm according to the typical local experience. A tendon diameter of 12.7 mm and tendon spacing of 0.8 m were tentatively used. A tentative distribution angle of 30° was used.

3.3. Effect of Slab Thickness

The effect of concrete slab thickness on the stress distribution was analyzed. The diameter of the tendon was 12.7 mm, the tendon distribution angle was 30°, and tendon spacing in the longitudinal direction was 800 mm. The slab thickness varied from 140 to 240 mm with an interval of 20 mm. The stress levels in the longitudinal and transverse directions were obtained, and are shown in Figure 3. Both the longitudinal and transverse stresses decreased with an increase in slab thickness. The decreased degree of longitudinal stress was higher than that of the transverse stress, because the tendon distribution angle was smaller than 45°. This aligns with expectations—a thicker slab has an increased cross sectional area, which reduces the average stress level.

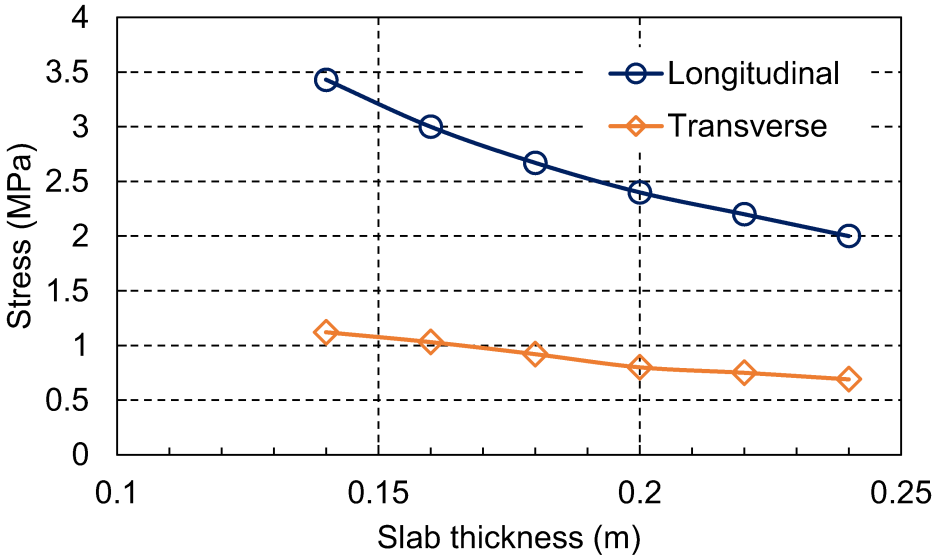

Figure 3. The effect of concrete slab thickness on the stress level.

3.4. Effect of Prestressed Tendon Diameter

When the tendon spacing is determined, the prestress reinforcement ratio is mainly dependent on the tendon diameter. Three tentative tendon diameters were selected for the parametric study: 9.5 mm, 12.7 mm, and 15.2 mm. The concrete slab thickness, tendon angle, and tendon spacing were 20 cm, 30°, and 800 mm, respectively. Both the longitudinal and transverse stresses increased with tendon diameter, as shown in Figure 4. A bigger tendon diameter means a higher prestressed force applied on the concrete, and therefore, a higher stress level. The magnitude of increase of the longitudinal stress was higher than the transverse stress.

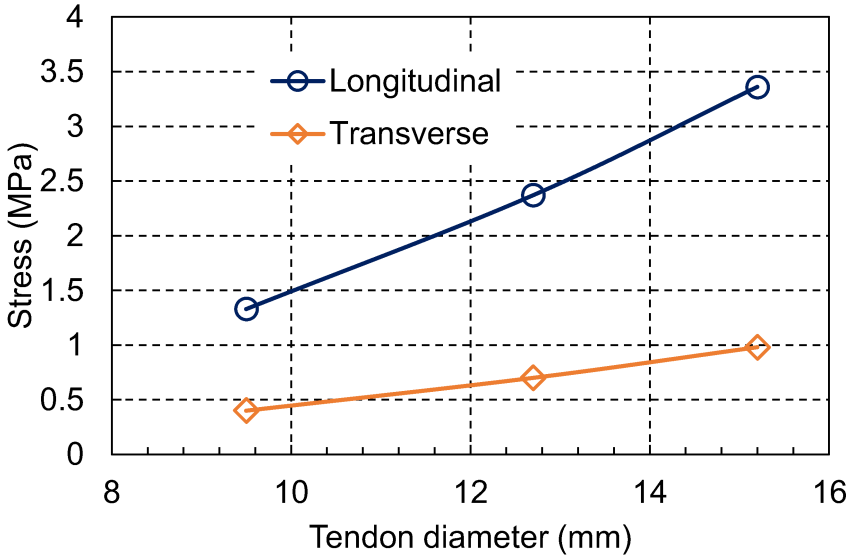

Figure 4. The effect of prestressed tendon diameter on the stress level in concrete slab.

3.5. Effect of Tendon Distribution Angle and Spacing

The tendon distribution angle greatly affects the ratio of longitudinal stress and transverse stress. A higher tendon distribution angle is expected to bring higher longitudinal stress and lower transverse stress. Typically, a higher longitudinal stress is desirable because it demands a smaller tendon distribution angle. A low tendon distribution angle would be more challenging to design and construct the anchorage area. In addition, the transverse prestress is beneficial to resist the traffic related slab deformation; therefore, the tendon distribution angle from 25° to 45° with an interval of 5° was used for the parametric study. In terms of the spacing, three tentative values were used: 0.5 m, 0.8 m, and 1.0 m. Figure 5 displays the effect of the tendon distribution angle and tendon spacing on the stress level in the concrete slab. As expected, the longitudinal stress increased and the transverse stress decreased with an increase in tendon distribution angle. It is was observed that the transverse stress was generally linearly correlated with the tendon distribution angle, and the longitudinal stress was not; this is mainly due to the variable α in the Equations (6) and (7). The dependent variable for the longitudinal stress, $cos(\alpha)/tan(\alpha)$, is more complicated than that for the transverse stress, $cos(\alpha)$. In terms of the effect of tendon spacing on the stress level in the concrete slab, it can be determined from Figure 5 that an increase in space from 0.5 m to 1.0 m would result in lower longitudinal and transverse stresses. This is paralleled with expectation since a larger spacing results in a lower reinforcement rate and therefore, lower load on the concrete slab.

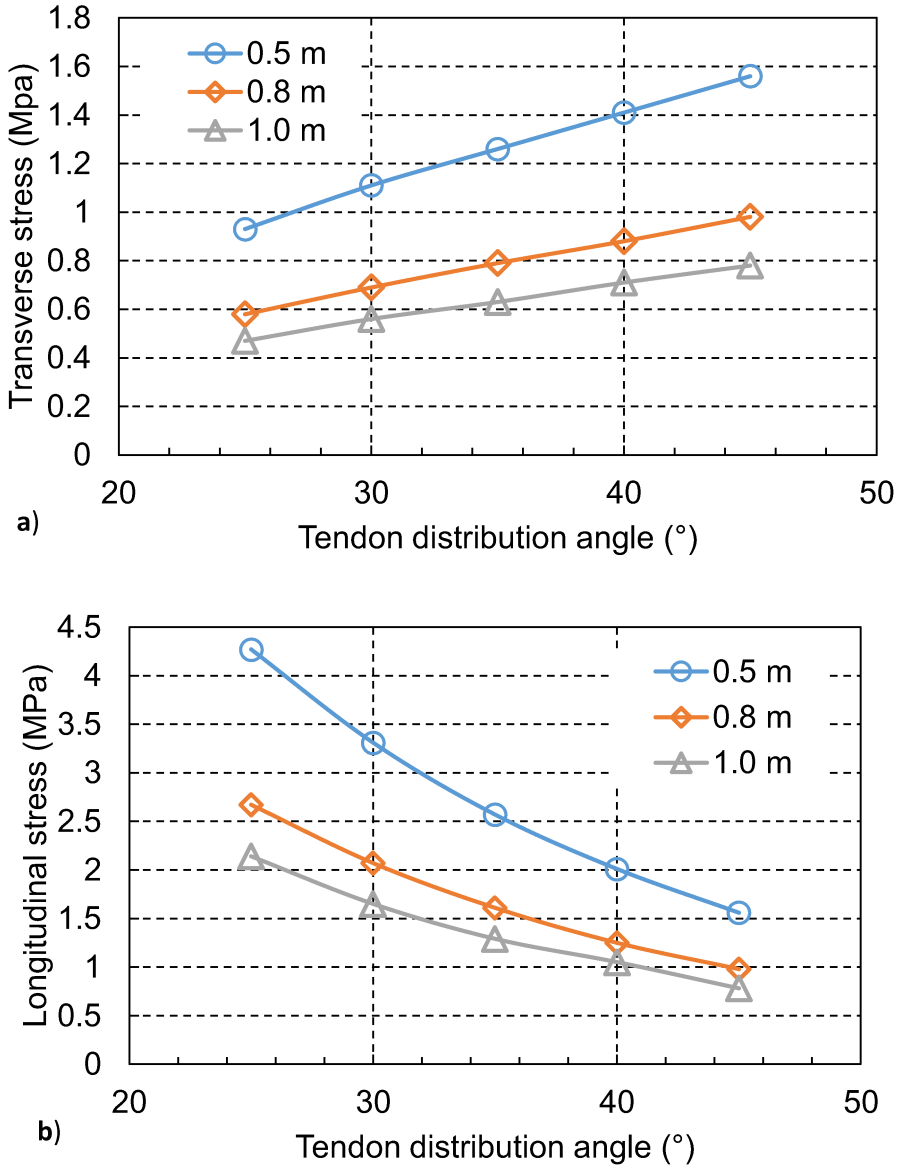

Figure 5. The effect of tendon distribution and spacing on the stress level in concrete slab: (**a**) longitudinal stress; and (**b**) transverse stress.

3.6. Buckling of Concrete Slab

Temperature differential at the top and bottom of concrete slab is very common. The maximum temperature differential which causes buckling is known as the critical temperature differential. For a concrete slab, the critical temperature can be expressed as [27]:

$$\Delta T_{cr} = \frac{H^2\pi^2}{12(1+v)\alpha}\left(1+\frac{1}{\lambda^2}\right) + \frac{K(1-v)w}{E_c H\alpha\pi^2}\frac{1}{1+\lambda^2} \quad (8)$$

where,

H = the thickness to width ratio;
E_c = elastic modulus of concrete;
K = the coefficient of subgrade;
w = the width of concrete slab;
v = the Poisson's ratio of concrete;

λ = the length to width ratio;
α = the linear expanding coefficient.

$$K = \frac{2\varphi(1-v^2)\pi \times 1.77}{4 \times 0.4} K_r \quad (9)$$

where,

K_r = the resilient modulus of the subgrade;
φ = the radius of the rigid plate (cm), 15 cm.

Since the prestressing applied on the concrete slab has a similar effect as the temperature differential the prestressing value can be converted to the equivalent temperature differential, as follows:

$$\Delta T_y = F_l(1+v)/(\alpha E) \quad (10)$$

where,

ΔT_y = the equivalent temperature differential caused by prestressing;
F_l = the prestress level in the concrete slab.

3.7. Parametric Study on Buckling

In practice, some typical values for the parameters in Equations (9) and (10) have been used. Typically, the length to width ratio is between 1.0 and 3.0, the thickness to width ratio is between 1:45 and 1:30, and the compressive strength of concrete is between 15 and 40 MPa. Tentatively, we take λ, H, and K to be 1.0, 1/35, and 1×10^{-3} N/mm^3, respectively.

The effect of some individual parameters on the critical temperature differential was analyzed. Figure 6 displays the effect of various factors on the critical temperature differential in the concrete slab. All of the four investigated parameters have significant influences on the critical temperature differential. It was determined that an increase in resilient modulus of subgrade results in a lower critical temperature differential. In terms of the dimensional effect, an increase in length to width ratio results in a lower critical temperature differential, while the thickness to width ratio exhibits an opposite effect. The values of $v = 0.15$, $\alpha = 1 \times 10^{-5}$ m/°C, $H = 0.02$, $\lambda = 30$, $E = 16{,}000$ MPa were used to calculate the critical temperature causing buckling; according to Equation (8), the critical temperature differential was calculated to be 48.2 °C. This value is higher than the maximum temperature range within a day, therefore, the buckling due to natural temperature change would not occur in this case.

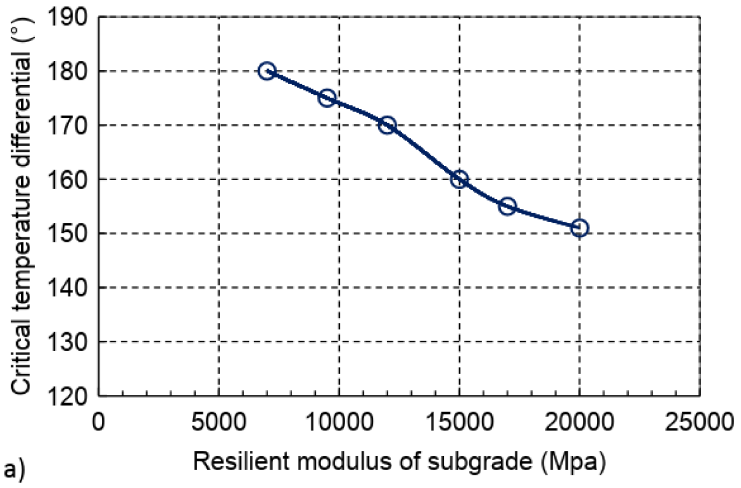

Figure 6. *Cont.*

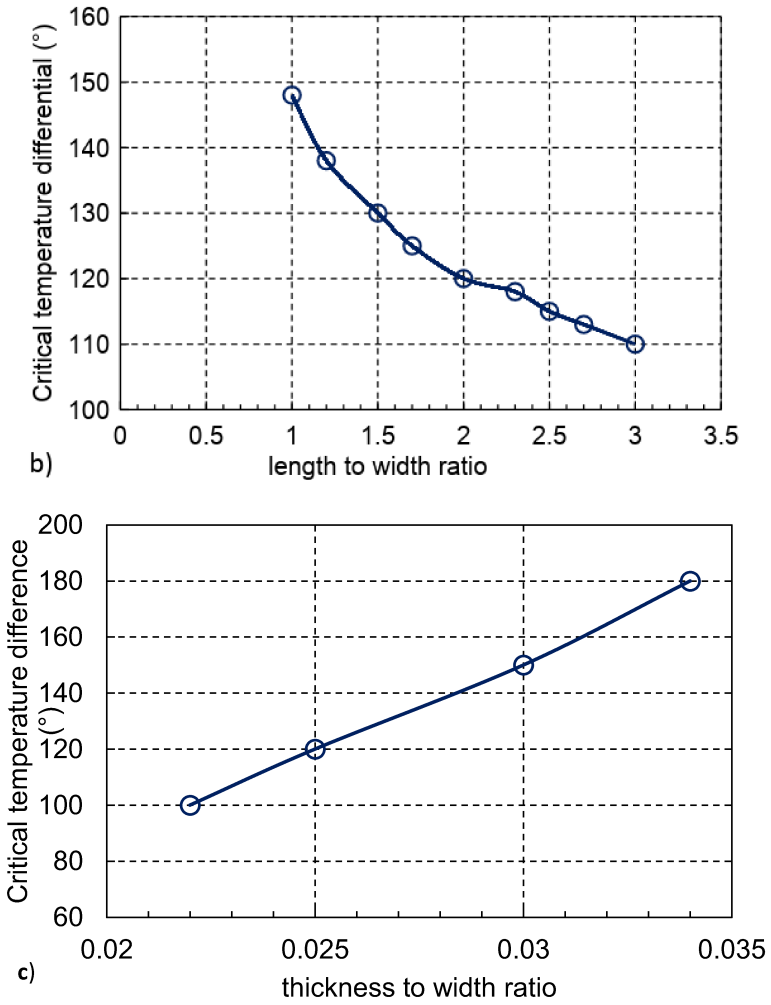

Figure 6. The effect on the critical temperature differential: (**a**) resilient modulus of subgrade; (**b**) length to width ratio; and (**c**) thickness to width ratio.

4. Design of Demonstrative Concrete Pavement Section

The trial pavement section was 150 m in length, 6 m in width, and 20 cm in thickness. The base layer was cement stabilized gravels and the cushion layer was recycled concretes. The thickness of both the base layer and the cushion layer was 20 cm, the resilient modulus was 40 MPa, and the diameter of the prestressed tendon was 12.7 mm. The design of the oblique prestressed concrete pavement is shown in Figure 7. Two layers of tendons were obliquely distributed with an angle in the longitudinal direction, as seen in Figure 7a. The prestressing was applied in the center of the concrete slab so that there is no eccentric force. In addition, spiral reinforcement was applied on the side to strengthen the anchorage area (seen in Figure 7a) and regular steel reinforcement was applied on the top and bottom of the concrete slabs (seen in Figure 7b). The design of the prestressed concrete pavement is based on the fracture criteria and fatigue criteria. The details are described below.

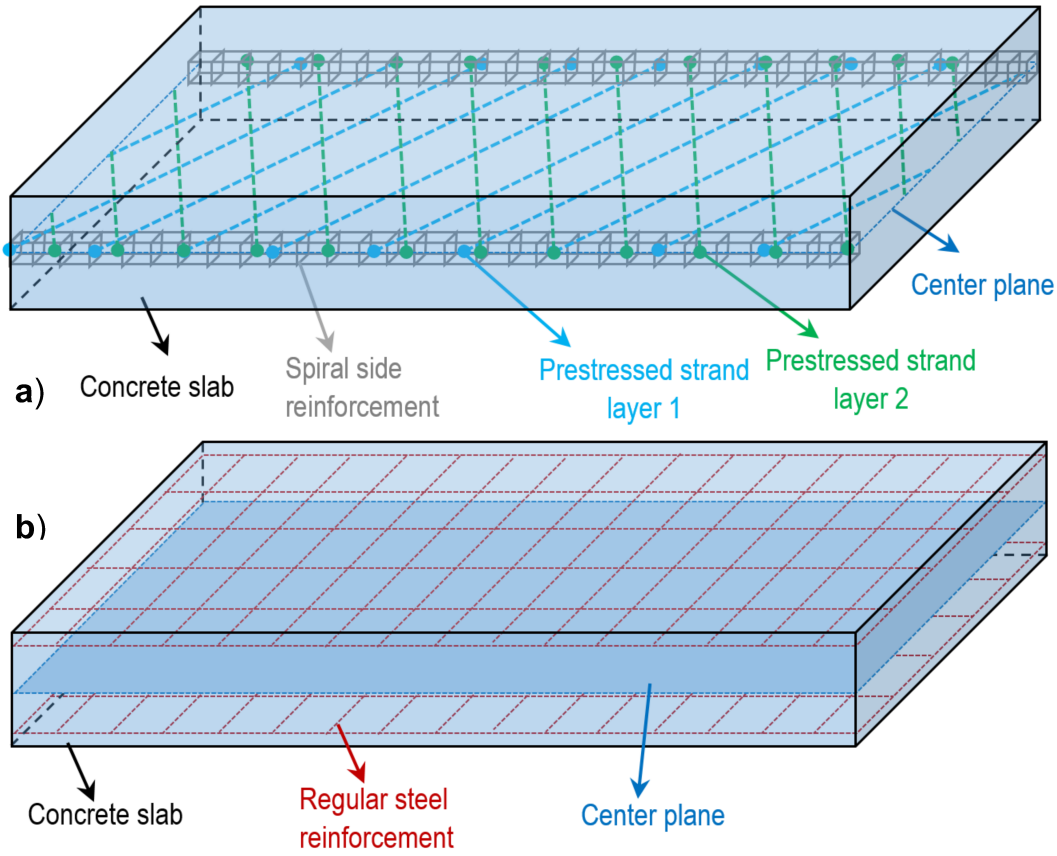

Figure 7. Illustration of the design of demonstrative oblique prestressed concrete pavement: (**a**) the distribution of oblique prestressed strands and side reinforcement; (**b**) the distribution of regular steel reinforcement.

4.1. Stress within the Concrete

4.1.1. Fracture Criteria

The stress within the concrete slab is determined by three components: the traffic induced stress, temperature and moisture induced stress, and the friction stress with base layer. If the combined stress is higher than the tensile strength of concrete, fracture failure will occur. Therefore, the following equation should be valid [28]:

$$\gamma(\sigma_{L,r} + \sigma_{\Delta Tr}) + \sigma_F - \sigma_{pL} \leq f_r \tag{11}$$

where,

f_r = the tensile strength of concrete;
$\sigma_{\Delta Tr}$ = temperature induced stress;
$\sigma_{L,r}$ = traffic induced stress;
σ_F = friction related stress;
σ_{pL} = effective prestress in longitudinal direction;
γ = coefficient of reliability.

The load induced stress level at the critical locations is expressed as:

$$\sigma_{L,r} = k_f k_c \sigma_L \tag{12}$$

where,

σ_L = initial load induced stress;
k_f = coefficient for fatigue cracking;
k_c = coefficient for the impact of eccentric and dynamic loading.

The temperature induced stress level is expressed as:

$$\sigma_{\Delta Tr} = k_t \sigma_{\Delta t} \tag{13}$$

where,

k_t = coefficient of cumulative fatigue stress;
$\sigma_{\Delta t}$ = the thermal stress, expressed as:

$$\sigma_{\Delta t} = \frac{E_c \alpha_c \Delta T}{2(1-\nu_c)} \tag{14}$$

where,

E_c = elastic modulus of concrete (MPa);
α_c = expansion coefficient of concrete;
ν_c = Poisson's ratio;
ΔT = the temperature gradient along the thickness (°C).

4.1.2. Fatigue Criteria

The fracture criteria is used to ensure the stress within the concrete slab is not higher than the tensile strength of concrete. However, fatigue crack may occur even if the stress level is lower than the tensile strength due to repeated loading. According to the specification of prestressed concrete pavement in China, the fatigue crack of concrete slab is a criterion of design. The PCA fatigue model was adopted in this study [29], expressed as:

$$\rho_\sigma = 0.972 - 0.08281 lg(N) \tag{15}$$

where,

N = the fatigue life;
ρ_σ = the ratio between the stress level to the tensile strength of concrete.

$$\rho_\sigma = \frac{\gamma(\sigma_{L,r} + \sigma_{\Delta Tr}) + \sigma_F - \sigma_{pL}}{\sigma_{pL} + f_r} \tag{16}$$

Therefore, the required prestress level in longitudinal direction should be:

$$\sigma_{pL} \geq \frac{\gamma(\sigma_{L,r} + \sigma_{\Delta Tr}) + \sigma_F}{1+\rho_\sigma} - \frac{\rho_\sigma}{1+\rho_\sigma} f_r \tag{17}$$

4.2. Stress in Anchorage Area

Anchorage area could be venerable because the force is applied in a small area. There are two types of failures for the anchorage area: one is the regional concrete failure which occurs in the small area right under the base plate, and the other is the tensile failure of concrete along with the tensioning direction which usually occurs over a much wider area [30]. The regional failure within the anchorage area was analyzed in this study, as it is a more critical concern. The regional stress level should meet the requirement below [31]:

$$F_l \leq 0.9\left(\beta_c \beta_l f_c + 2\alpha \rho_v \beta_{cor} f_y\right) A_{ln} \tag{18}$$

where,

F_l = the regional stress level in the anchorage area;
β_c = the strength coefficient of concrete;
β_l = the increase coefficient of concrete in compression;
f_c = the design compressive strength of concrete;
α = the reduction coefficient due to spiral reinforcement;
ρ_v = the volume proportion of spiral reinforcement;
f_y = the tensile strength of spiral steels;
A_{ln} = the area of concrete under compression.

4.3. Stress Analysis

4.3.1. Stress Analysis on Concrete

Concrete slab dimensions were selected to be L = 100 m, w = 4.5, t = 20 cm, the tensile strength of concrete f_r = 5 MPa, elastic modulus E_c = 25,500 MPa, coefficient of reliability γ = 1.08, Poisson's ratio v_c = 0.15, expansion coefficient $\alpha_c = 1 \times 10^{-5}/^{\circ}\mathrm{C}$, and temperature gradient ΔT = 0.9 °C/cm.

According to the fracture criteria,

$$r = 0.537h\left(\frac{E_c}{E_t}\right)^{\frac{1}{3}} = 0.537 \times 0.2 \times \left(\frac{30,000}{165}\right)^{\frac{1}{3}} = 0.61$$

$$\sigma_L = 0.077r^{0.60}\,\mathrm{h}^{-2} = 0.077 \times 0.61^{0.60} \times 0.2^{-2} = 1.43\ \mathrm{MPa}$$

$$\sigma_{L,r} = k_f k_c \sigma_L = 1.69 \times 1.2 \times 1.43 = 2.90\ \mathrm{MPa}$$

$$\sigma_{\Delta T} = \frac{E_c \alpha_c \Delta T}{2(1 - v_c)} = \frac{25,500 \times 1 \times 10^{-5} \times 0.9 \times 20}{2 \times (1 - 0.15)} = 2.7\ \mathrm{MPa}$$

$$\sigma_F = \mu\rho\chi = 0.8 \times 0.024 \times 50 = 0.96\ \mathrm{MPa}$$

$$\text{Then } \sigma_{py} \geq \gamma(\sigma_{L,r} + \sigma_{\Delta Tr}) + \sigma_F - f_r = 1.08 \times (3.78 + 2.7) + 0.96 - 5 = 2.96\ \mathrm{MPa}$$

This means that the prestress applied on the concrete slab should be higher than 2.96 MPa to prevent fracture distress.

According to the fatigue criteria,

$$N = \frac{N_e}{t} = \frac{100 \times 10^4}{30} = 3.3 \times 10^4$$

$$\rho_\sigma = 0.972 - 0.08281 lgN = 0.972 - 0.08281 lg\left(3.3 \times 10^4\right) = 0.6$$

$$\text{Then, } \sigma_{py} \geq \frac{\gamma(\sigma_{L,r} + \sigma_{\Delta Tr}) + \sigma_F}{1 + \rho_d} - \frac{\rho_d}{1 + \rho_d} f_r = \frac{1.08 \times (3.78 + 2.7) + 0.96}{1 + 0.6} - \frac{0.6}{1 + 0.6} \times 5 = 3.10\ \mathrm{MPa}$$

This means that the effective prestress applied on the concrete slab should be higher than 3.1 MPa to prevent fatigue failure. Therefore, the prestress level should be higher than 3.10 MPa taking into account both the fracture and fatigue criteria.

4.3.2. Determine Tendon Spacing

The tensile strength of the tendon was 1860 MPa. The total loss of prestress in the concrete slab was about 20% [32]. The longitudinal spacing can be calculated as:

$$L = \frac{2(\sigma_{con} - \sigma_1) \times A_p \times cos\alpha}{\sigma_{py} \times h \times tan\alpha} = \frac{2 \times 1116 \times 98.7 \times cos30}{3.10 \times 200 \times tan30} = 532.98\ \mathrm{mm}$$

Therefore, the spacing in longitudinal direction was selected as 500 mm.

4.3.3. Verification

According to

$$0.95\sigma_s \leq \sigma_L + \sigma_{\Delta T} \leq 1.03\sigma_s$$

$$\sigma_s = f_{cm} + \sigma_{Py} - \sigma_F = 3.33 + 3.10 - 0.96 = 5.47 \text{ MPa}$$

$$\sigma_{pr} + \sigma_{\Delta T} = 2.90 + 2.7 = 5.60 \text{ MPa}$$

$$0.95 \times 5.47 = 5.20 \text{ MPa} \leq 5.60 \text{ MPa} \leq 1.03 \times 5.47 = 5.63 \text{ MPa}$$

Therefore, the distribution angle of 30° and longitudinal spacing of 500 mm can meet the requirement according to the stress analysis. The effective prestressing in the longitudinal direction was 3.1 MPa.

4.4. Regional Stress Analysis in Anchorage Area

The diameter of the tendon was 12.7 mm, the dimension and thickness of the base plate were 80 mm × 80 mm and 14 mm, respectively, and the compression area was 160 mm × 200 mm. HPB235 steel was used in the spiral reinforcement, and the spacing of the steel was 40 mm. According to Equation (18), the regional stress was analyzed below:

$$F_l = 1.2\sigma_{con}A_p = 1.2 \times 0.75 \times 1860 \times 98.7 = 165.22 \text{ KN}$$

$$A_b = 160 \times 200 = 32,000 \text{ mm}^2$$

$$A_l = \frac{\pi}{4}(\alpha + 2\delta)^2 = \frac{\pi}{4}(50 + 2 \times 14)^2 = 4778 \text{ mm}^2$$

$$A_{ln} = 4778 - 98.7 = 4679.3 \text{ mm}^2$$

$$\beta_l = \sqrt{\frac{A_b}{A_l}} = 2.59 \quad \beta_c = 1 \quad f_c = 16.7$$

$$\alpha = 0.5 \text{ m} \quad f_y = 210 \text{ MPa} \quad A_{ssl} = 78.54 \text{ mm}^2 \quad d_{cor} = 100 \text{ mm}$$

$$\rho_v = \frac{4A_{ssl}}{d_{corS}} = \frac{4 \times 78.54}{100 \times 40} = 0.079$$

$$A_{cor} = \frac{\pi}{4}{d_{cor}}^2 = \frac{\pi}{4} \times 100^2 = 7854 \text{ mm}^2 < A_b$$

$$0.9\left(\beta_c\beta_l f_c + 2\alpha\rho_v\beta_{cor}f_y\right)A_{ln}$$
$$= 0.9 \times (1 \times 2.59 \times 16.7 + 2 \times 0.5 \times 0.079 \times 1.28 \times 210) \times 4679.3$$
$$= 271.58 \text{ KN} > F_l$$

Therefore, the regional stress in the anchorage area is sufficient.

5. Materials and Preparation

5.1. Cement and Aggregates

According to the standard for Unbounded Prestressed Concrete Structure in China [31], the strength grade of the concrete used in pavement should be higher than C30. Other requirements of the cement include low shrinkage and creep, rapid hardening, and high early-stage strength. The shrinkage and creep of concrete will cause prestress loss so that the effective stress within the concrete slab would be compromised. On the other hand, the rapid hardening and high early-stage strength allows for the application of the prestress soon after the construction and reduces shrinkage

crack. Therefore, PO 425 silicate cement with a strength grade of C35 was used in this study to fabricate the prestressed cement concrete.

Coarse aggregates and sands are an important composition of cement concrete. Coarse aggregates with regular shape and good angularity were selected to prepare the cement concrete in this study, thus the use of flat or elongated aggregates was limited. The biggest aggregate size used was 31.5 mm and medium sand with a fineness modulus of about 2.5–3 was used as the fine aggregates. The gradation of the coarse aggregates and sands are shown in Table 1.

Table 1. The gradation of coarse and fine aggregates.

Aggregates	**Mesh Size (mm)**		**2.4**	**4.8**	**9.5**	**16.0**	**19.0**	**26.5**	**31.5**
Coarse	Cumulative retained (%)	Upper limit	100	100	90	75	60	35	5
		Lower limit	95	90	75	60	40	20	0
	Mesh size (mm)		**0.15**	**0.30**	**0.60**	**1.18**	**2.36**	**4.75**	-
Fine	Cumulative retained (%)	Upper limit	100	92	70	50	25	10	-
		Lower limit	90	70	41	10	0	0	-

5.2. Concrete Design

After the raw materials were prepared, concrete design was the next step. Concrete design mainly refers to the selection of proper fractions for each composition including water, cement, sand, coarse aggregates, and superplasticizer. Water–cement (W/C) ratio is the most important index affecting the workability and mechanical performance in concrete design. A preliminary design was carried out according to the concrete design specification in China, in which the W/C ratio was 0.39 and the sand to coarse aggregate (S/A) ratio was 0.47 and the two parameters were adjusted by plus and minus a small value [23]. Initially, three tentative W/C ratios were selected according to the specification and preliminary calculation, as seen in Table 2. The amounts of other compositions were selected correspondingly for each W/C ratio.

Table 2. The gradation of coarse and fine aggregates.

Compositions	**Design 1**	**Design 2**	**Design 3**
Water–cement ratio	0.35	0.39	0.43
Sand to coarse aggregate ratio	0.49	0.47	0.45
Cement mass percent	17.9	19.7	20.3
Sand mass percent	24.4	23.3	22.2
Coarse aggregates mass percent	49.6	49.1	50.0
Water mass percent	7.8	7.8	7.3
Superplasticizer mass percent	0.2	0.2	0.2

The compressive strength and the slump of the concrete based on different designs were tested, and are shown in Figure 8. With an increase in W/C ratio, the slump of fresh concrete increased while the 7-day and 28-day compressive strength of hardened concrete decreased (this was expected). It is worth noting that the 7-day strength can arrive at about 102%, 96%, and 93% of the design strength for the three designs, respectively. A W/C ratio of 0.39 was selected to balance the workability and compressive strength.

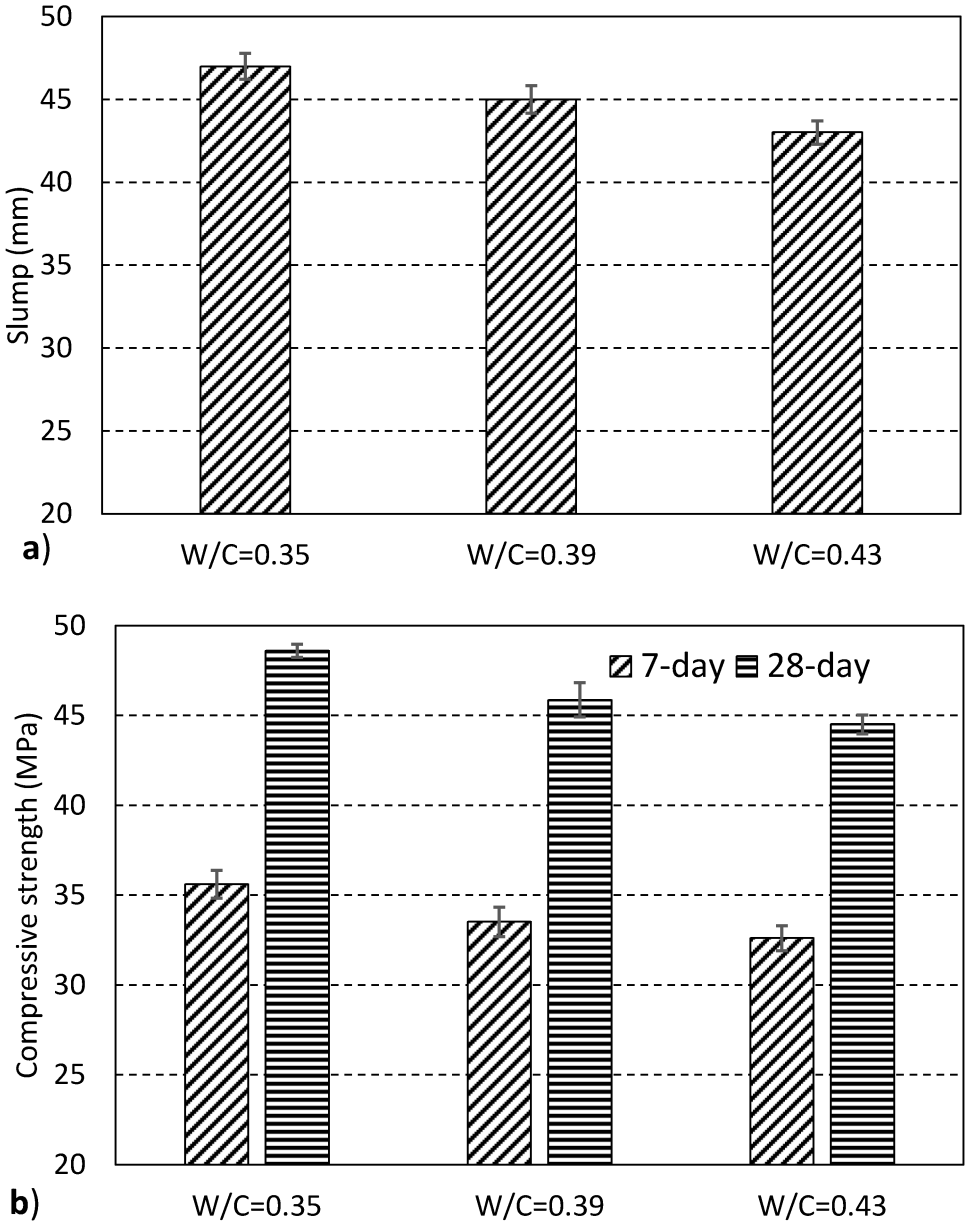

Figure 8. The properties of the concrete at various W/C ratios: (**a**) slump of fresh concrete; and (**b**) 7-day and 28-day compressive strength of hardened concrete.

5.3. Prestressed Concrete Tendons

The prestressed tendons used in this study consisted of three parts: the prestressed wires, restrictive coating, and the paint cover. Seven high quality steel wires were included to form the tendon, with the diameter of the steel tendon being 12.7 mm. High-density polyethylene was used as the restrictive coating to prevent damage of wires during transport, storage, and placement. Asphalt or grease was used as the paint cover to reduce the friction between the tendons and concrete during prestressing. The design tensile strength of the prestressed tendons was 1860 MPa.

5.4. Anchorage

The anchorage is an important part which determines the success of the prestressing. There are two anchors in an anchorage system: the fixing end anchor and the tensioning anchor. An extruding anchor and jaw vice anchorage were used for the fixing end anchor and tensioning anchor, respectively.

The diameter of the extruding anchor was 50 mm, the size and thickness of the bearing plate were 80 mm × 80 mm, 14 mm, respectively, and the size of the compressive section was 160 mm × 200 mm. The post-tension method was applied in this study, so the anchors were placed in the concrete during the casting.

6. Construction of Demonstrative Pavement Section

6.1. Side Formwork

Steel side formwork was used in the construction. Cement mortar was placed in the low-lying area to make sure the bottom of the side formwork contacted well with the base layer. After installing the formwork, the template junctions and the inside were examined, and the height difference between two templates in the joint area were measured to be no higher than 3 mm. The reserved length of the prestressed reinforcement ranged from 40 to 60 cm. Some holes were reserved on the formwork to allow the prestressed tendons to go through. It is noteworthy that the height of the tendons should be the same so that uniform stresses can be applied.

6.2. Sliding Layer

A sliding layer was paved on the top of the base layer before placing the concrete pavement. Common materials include asphaltic felt, geotextiles, and polyethylene layers. The material and construction method followed the specification for prestressed concrete pavement in China [33]. In this study, fine granular materials with a maximum size of 0.3 mm were initially placed with a thickness of 10 mm and then geotextiles were placed on the top of the granular materials.

6.3. Distribution of Tendons and Tensioning

Prestressed tendons were applied in the middle of the concrete slabs. The angle between the steel tendon and the road direction was 30°, so the angle between the tendons in two layers was 60°, as shown in Figure 9. The tensioning was applied via two steps: the first tensioning was applied to 30% of the design strength (1860 MPa) of the tendon after the 12 h of the concrete casting, and the second tensioning was applied to 105% of the design strength after 7 days of the concrete placement. The distance between neighboring tendons was 0.5 m. The grade of the anchor seal concrete was higher than that in the pavement, which means higher than C35. The spiral indirect reinforcement was applied using Φ10 smooth steel (HPB235). The spacing and radius of the screw were 30 mm and 40 mm, respectively. Four anti-splitting steel bars (Φ8) with a spacing of 60 mm were arranged.

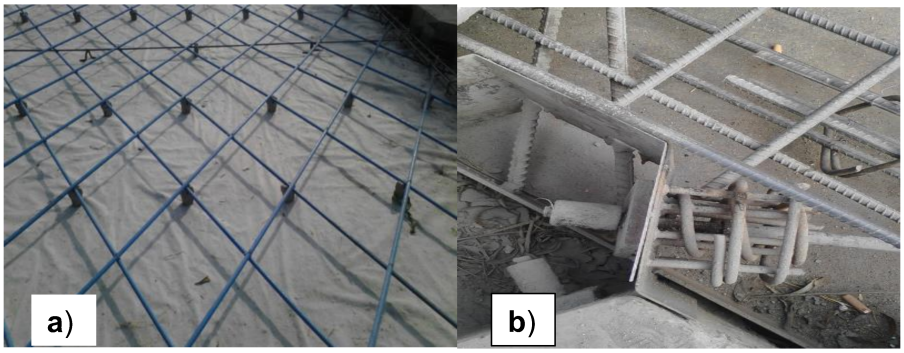

Figure 9. (**a**) The distribution of the prestressed tendons; and (**b**) the fixed end anchor.

6.4. Reinforcement at Slab Top and Bottom

Because the prestressed reinforcement was only applied to the middle part of the concrete slabs (in other words, the top and bottom were un-reinforced), an unbalanced force within the concrete slab

was produced. Given this, reinforcement using Φ12 regular steel bars (with a spacing between the bars of 250 mm) was applied at the top and bottom parts of the concrete slab, as seen in Figure 10. In addition, steel reinforced sleeper beam was placed between the concrete slab and the base layer to ensure good load transfers.

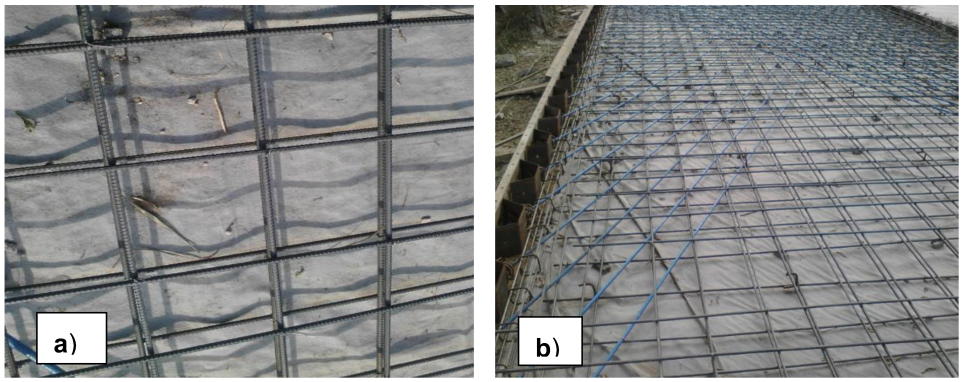

Figure 10. The distribution of reinforcement: (**a**) two-layer regular steel reinforcement; and (**b**) the prestressed reinforcement and the regular reinforcement.

6.5. Concrete Placing and Curing

The placing of concrete was completed continuously to avoid unnecessary joints. Vibration was applied during the placing to achieve high density. The side formwork and the prestressed tendons were not touched during the vibration to avoid displacement. The curing started right after the placing of concrete slabs. Geotextiles were used to cover the top of the concrete pavement and water was spread. The curing process lasted 14–21 days until the tensile strength of the concrete reached 80% of the design value.

6.6. Pavement Monitoring System

After the construction of the concrete pavement and the application of prestressing, the stress condition of the concrete pavement was monitored. For this purpose, a prestressed tendon anchorage dynamometer and piezoelectric sensor were placed in the base layer of the pavement. The schematic distribution of the pavement monitoring system is shown in Figure 11.

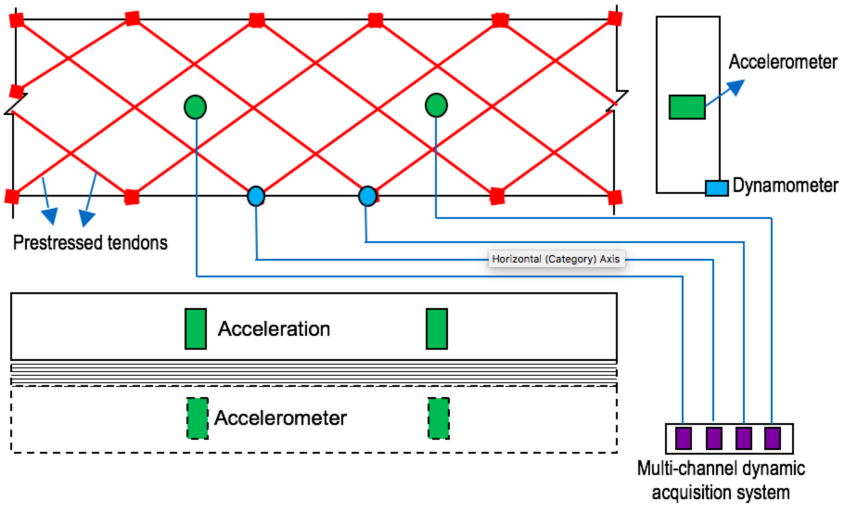

Figure 11. Schematic multi-views of the inclined prestressed concrete pavement monitoring system.

7. Summary and Conclusions

This paper presented a detailed design and construction of oblique prestressed concrete pavement. Prestressed tendons were distributed obliquely with the longitudinal direction so that prestress was applied in both the transverse and longitudinal direction. Compared to simple prestressing in the longitudinal direction or precast prestressed concrete pavement, the oblique prestressed concrete pavement allowed a much higher joint spacing. The design of prestressed concrete pavement included the selection of raw materials, design of cement concrete, anchorage area, size and distribution of prestressed tendons, stress analysis within the concrete slab, sliding layer, side reinforcement, and regular reinforcement at top and bottom. A pavement monitoring system was embedded in the concrete pavement to survey the condition of the pavement after traffic opening. Some findings of the study can be summarized as below:

1. The cement concrete was designed based on the compressive strength and workability to meet the requirement of prestressed concrete in China;
2. The possible buckling of concrete slab due to temperature change or prestressing was evaluated and it was determined that buckling would not occur under the natural temperature change in China;
3. The required prestress applied on concrete slabs was obtained based on fracture criteria and fatigue criteria and the prestressed tendon spacing was obtained based on the stress analysis;
4. The effect of slab thickness, tendon diameter, tendon distribution angle, and tendon spacing on the stress level within the concrete slab were analyzed in detail;
5. Spiral indirect reinforcement on the side was applied to strengthen the anchorage area and regular reinforcement was applied on the top and bottom of the concrete slabs to improve the stress condition;
6. The design of the anchorage area was verified based on regional stress analysis;
7. The step-by-step construction of the oblique prestressed concrete pavement was described and the demonstration road section has performed well over the three years since traffic opening.

Author Contributions: Ling Yu and Xu Yang conceived and designed the experiments; Xu Yang also help finalize the manuscript; Xiaohui Yan and Xiaowei Zhang performed the experiments and wrote the draft of the paper; Ting Zhao helped improve the format and English of the manuscript; Julian Mills-Beale and Cong Duan helped improve the paper in paper organization and discussion based on his professional background in pavement engineering.

Conflicts of Interest: The authors declare no conflict of interest.

References

1. Hossain, M.; Hancock, J.; Wu, Z. Cross Tensioned Concrete Pavement. *J. Transp. Eng.* **2003**, *129*, 427–433. [CrossRef]
2. Sargious, M.; Wang, S.K. Design of Prestressed Concrete Airfield Pavements under Dual and Dual Tandem Wheel Loading. *J. Prestress. Concr. Inst.* **1971**, *16*, 19. [CrossRef]
3. Sargious, M.; Wang, S.K. Economical Design of Prestressed Concrete Pavements. *J. Prestress. Concr. Inst.* **1971**, *16*, 64. [CrossRef]
4. Sargious, M. Performance of Transverse Joints in Prestressed and Reinforced-Concrete Airfield Pavements. *J. Am. Concr. Inst.* **1978**, *75*, 359–366.
5. Merritt, K.D.; Tyson, S.S. Precast Prestressed Concrete Pavement Applications in the USA. In *Proceedings of the First International Conference on Recent Advances in Concrete Technology*; Amde, A.M., Sabnis, G., Tan, J.S.Y., Eds.; Destech Publications, Inc.: Lancaster, PA, USA, 2007; pp. 457–470.
6. Zhang, D.; Xu, X.; Li, N.; Han, W. Research on the Design Method of Diagonal Post-Tensioned Prestressed Jointless Cement Concrete Pavement. In Proceedings of the ICCTP 2011: Towards Sustainable Transportation Systems, Nanjing, China, 14–17 August 2011; American Society of Civil Engineers: Reston, VA, USA, 2011.
7. El-Reedy, M.A. *Advanced Materials and Techniques for Reinforced Concrete Structures*; CRC Press: Boca Raton, FL, USA, 2009.

8. Wieckowski, A.; Sznurawa, A. Structural Aspects of Airfield Runways with Concrete Pavements. In *Contemporary Challenges of Transport Systems and Traffic Engineering*; Macioszek, E., Sierpinski, G., Eds.; Springer International Publishing AG: Cham, Switzerland, 2017; pp. 39–52.
9. Li, N.; Han, S.; Yu, J.T.; Wang, H.F. Analysis of Bridge Deck Pavement Structure Interlayer Based on Different Interface Form. In Proceedings of the 10th International Conference of Chinese Transportation Professionals (ICCTP), Beijing, China, 4–8 August 2010; American Society of Civil Engineers: Reston, VA, USA, 2010.
10. Guo, C.; Zhang, M.; Wang, Z.; Wang, X. Analysis of Cross Tensioned Concrete Pavement Damage. In *Advances of Transportation: Infrastructure and Materials*; Wang, H., Liu, Y., You, Z., Eds.; Destech Publications, Inc.: Lancaster, PA, USA, 2006; Volume 2, pp. 893–899.
11. Han, S.; Chen, D.; Ling, C.; Zhang, D. Study on sliding layer of cross-tensioned concrete pavement. *Road Mater. Pavement Des.* **2015**, *16*, 518–535. [CrossRef]
12. Li, N.; Zhang, D.; Xu, X.; Han, W. Numerical Simulation on Cross-Tensioned Prestressed Concrete Pavement. In Proceedings of the Fourth International Conference on Transportation Engineering, Chengdu, China, 19–20 October 2013; American Society of Civil Engineers: Reston, VA, USA, 2013.
13. Tayabji, S. *Precast Concrete Pavement Implementation by US Highway Agencies*; The National Academies of Sciences, Engineering, and Medicine: Washington, DC, USA, 2015.
14. Kawamura, N.; Maekawa, R.; Morohashi, K.; Shiji, A.; Kamitani, K. Development of high durable grout for airport prestressed concrete pavement. In *Advances in Transportation Geotechnics II*; CRC Press, Taylor & Francis Group: Boca Raton, FL, USA, 2012; pp. 259–264.
15. Tomek, R. Advantages of Precast Concrete in Highway Infrastructure Construction. *Procedia Eng.* **2017**, *196*, 176–180. [CrossRef]
16. Syed, A.; Sonparote, R.S. Analysis of Prestressed Precast Concrete Pavement. *Mater. Today Proc.* **2017**, *4*, 9713–9717. [CrossRef]
17. Merritt, D.K.; McCullough, B.F.; Burns, N.H. Design-construction of a precast, prestressed concrete pavement for Interstate 10, El Monte, California. *PCI J.* **2005**, *50*, 18–27. [CrossRef]
18. Qu, B.; Weng, X.; Zhang, J.; Mei, J.; Guo, T.; Li, R.; An, S. Analysis on the deflection and load transfer capacity of a prefabricated airport prestressed concrete pavement. *Constr. Build. Mater.* **2017**, *157*, 449–458. [CrossRef]
19. Zhang, M.; Guo, C.; Lu, L.; Wang, X.; Wang, Z. Cross Tension Prestressed Concrete Pavements Temperature Stresses. In *Advances of Transportation: Infrastructure and Materials*; Wang, H., Liu, Y., You, Z., Eds.; Destech Publications, Inc.: Lancaster, PA, USA, 2016; Volume 2, pp. 947–954.
20. Naddafi, M.F.; Sadeghi, V. Finite Element Investigation of the Prestressed Jointed Concrete Pavements. *J. Fundam. Appl. Sci.* **2016**, *8*, 167–178. [CrossRef]
21. Kim, K.; Tia, M.; Greene, J. Evalution of Strauctural Behavior of Precast Prestressed Concrete Pavement with Finite Element Analysis. *Transp. Res. Rec.* **2016**, *2590*, 84–93. [CrossRef]
22. Melhem, H.; Kim, H.S. Damage detection in concrete by Fourier and wavelet analyses. *J. Eng. Mech.* **2003**, *129*, 571–577. [CrossRef]
23. China Academy of Building Research. *JGJ 55-2000 Specification for Mix Proportion Design of Ordinary Concrete*; China Building Industry Press: Beijing, China, 2001.
24. Yan, Y.; Liu, C.; Huang, W. Structural Design of Continuous Reinforced Concrete Pavement as Overlay. *J. China Foreign Highw.* **2005**, *5*. (In Chinese)
25. Zirakian, T.; Showkati, H. Experiments on Distortional Buckling of I-Beams. *J. Struct. Eng.* **2007**, *133*, 1009–1017. [CrossRef]
26. Wei, W.; Dong, D. Prestress Loss Calculation due to Anchor Deformation. *J. Archit. Sci. Eng.* **2007**, *24*, 86–90.
27. Wang, F. Study on the Structural Performace of Prestressed Highway Tunnel Pavement. Master's Thesis, Chang'an University, Xi'an, China, 2013. (In Chinese)
28. *GB50422, Engineering Technical Standard of Prestressed Concrete Pavement*; Ministry of Housing and Urban Construction: Beijing, China, 2007.
29. Hazaree, C.; Wang, K.; Ceylan, H.; Gopalakrishnan, K. Capillary Transport in RCC: Water-to-Cement Ratio, Strength, and Freeze-Thaw Resistance. *J. Mater. Civ. Eng.* **2011**, *23*, 1181–1191. [CrossRef]
30. Wu, J. The Design of Anchorage Area of Post-tensioning Concrete. Master's Thesis, Tongji University, Shanghai, China, 2007.

31. Zirakian, T.; Zhang, J. Elastic distortional buckling of singly symmetric I-shaped flexural members with slender webs. *Int. J. Struct. Stab. Dyn.* **2012**, *12*, 359–376. [CrossRef]
32. Yan, X. The Application of Oblique Prestressed Concrete Pavement Technology Research. Master's Thesis, Shenyang Jianzhu University, Shenyang, China, 2015.
33. Ministry of Housing and Urban-Rural Development of China. *GB 50422-2007: Technical Code for Engineerings of Prestressed Concrete Pavement*; China Plan Publishing: Beijing, China, 2007.